Chemical Science

ROYAL SOCIETY OF CHEMISTRY

EDGE ARTICLE

View Article Online
View Journal | View Issue

Cite this: *Chem. Sci.*, 2022, **13**, 14063

All publication charges for this article have been paid for by the Royal Society of Chemistry

Received 12th September 2022
Accepted 30th October 2022

DOI: 10.1039/d2sc05088a

rsc.li/chemical-science

Coordination unsaturation of vanadium nitride quantum dots boosts low-temperature aerobic oxidation of thiophenic sulfides†

Huawei Yang,[ab] Jiabao Bai,[a] Qinghua Zhang,[c] Lixia Yang,[a] Liangjiu Bai,[a] Donglei Wei,[a] Wenxiang Wang,[a] Ying Liang,[a] Lin Gu,[c] Hou Chen *[a] and Shaojun Guo *[b]

Aerobic oxidative desulfurization (AODS) promises a sustainable alternative technology for diesel desulfurization, which necessitates the efficient aerobic oxidation of thiophenic sulfides under mild conditions to minimize energy input, yet being longstandingly plagued by the grand challenge in low-temperature activation of triplet oxygen. Here we synthesize vanadium nitride quantum dots on graphene to controllably create coordination-unsaturated edge/corner V sites for boosting the AODS reaction. The catalyst activates the reaction at 70 °C, and is two orders of magnitude more active than the best V-based catalysts. We demonstrate through computational studies that the low-coordinated edge/corner V sites can effectively activate oxygen and adsorb sulfides to lower the activation barrier, dramatically enhancing the activity. The catalyst achieves deep AODS of real diesel at 80 °C with negligible attenuation in successive reuses, which highlights its attractive industrial potential. These findings provide scientific and practical insights to develop high-performance catalysts for a sustainable AODS process.

Introduction

In spite of the prosperity of renewable energies, diesel is still an indispensable high-energy-density fuel in the fields of long-range transportation and mechanical engineering, with a predicted daily consumption exceeding 30 million barrels in the next decade.[1] Nowadays, hydrodesulfurization is adopted in the refinery industry to eliminate the environmental hazards caused by combusting sulfur-containing diesels. However, traditional hydrodesulfurization suffers from poor conversion ability towards refractory sulfur compounds, such as dibenzothiophene (DBT) and its derivatives, requiring harsh reaction conditions (>350 °C, >6 MPa) to complete the sulfur removal, which results in ultra-high cost for energy consumption and equipment input. Aerobic oxidative desulfurization (AODS) is a promising alternative to HDS with excellent capability for removing refractory sulfides (Fig. S1†).[2,3] To avoid explosion risks and high energy consumption, AODS catalysts need to be active under low temperatures and atmospheric pressure. However, the ground state oxygen (O_2) is in the triplet state, which is chemically inert to most organic substances, thus putting forward a grand challenge for low-temperature reaction of O_2.[4–9]

Vanadium (V), molybdenum (Mo) and tungsten (W)-based metal oxides and polyoxometalates,[10–13] platinum (Pt) and copper (Cu)-based supported metal catalysts,[14,15] metal-free catalysts,[16,17] *etc.* have been proposed to be active in the AODS reaction. Among them, V-based oxide catalysts are potentially promising candidates because of their preferable activity and excellent stability, which drive the reaction at around 110 °C.[18,19] Since the activation of O_2 requires unsaturated V sites with strong adsorption and electron transfer capabilities, extensive efforts have been devoted to tuning the structure and surface properties of V oxides.[20] However, the enhancement of activity at low temperatures is still a grand challenge owing to the difficulty in modulating the electronic structure of V sites, which hinders V oxides from achieving energy efficiency at the industrial level.

Here we report the fabrication of vanadium nitride quantum dots (VN QDs) on a graphene sheet, controllably creating coordination-unsaturated edge/corner V sites for the low-temperature AODS reaction. We show that the catalyst is two orders of magnitude more active than the best V-based catalysts reported so far, and catalyzes the reaction at 70 °C. By combining kinetic analyses, advanced characterization and first-principles calculations, we assess how the size effect determines the catalytic activity and thereby identify that the coordination unsaturated edge/corner V species of VN QDs are

[a]School of Chemistry and Materials Science, Ludong University, Yantai, 264025, P. R. China. E-mail: chenhou@ldu.edu.cn

[b]School of Materials Science and Engineering, Peking University, Beijing, 100871, P. R. China. E-mail: guosj@pku.edu.cn

[c]Institute of Physics, Chinese Academy of Sciences, Beijing, 100190, P. R. China

† Electronic supplementary information (ESI) available: Experimental details and supplementary data. See DOI: https://doi.org/10.1039/d2sc05088a

the most reactive to boost low-temperature activity. With atmospheric air under normal pressure as the oxygen source, we realize the complete aerobic conversion of all sulfides in diesel at an unprecedented low temperature of 80 °C, achieving ultra-deep desulfurization of diesel with extremely low energy consumption, suggesting the application potential of the catalyst for AODS at the industrial level.

Results and discussion

Synthesis and structural characterization of VN-QDs/rGO

VN QDs/rGO was synthesized *via* a two-step procedure. Firstly, a homogeneous precursor aqueous solution containing NH_4VO_3 and graphene oxide (GO) nanosheets was freeze-dried to form a sponge. Subsequently, VN QDs/rGO was obtained by annealing the precursor at 800 °C under an NH_3/Ar (4 : 6) atmosphere. For comparison, VN nanoparticles and V_2O_5 nanowires supported on graphene were also synthesized (denoted as VN NPs/rGO and V_2O_5/GO, respectively, Fig. S2 and S3†). The loading amount of V in VN QDs/rGO is determined to be 2.85 wt% *via* inductively coupled plasma optical emission spectrometry (ICP-OES, Table S1†). As demonstrated by transmission electron microscopy (TEM), the as-prepared material maintains the 2D structure of the original GO sheets (Fig. 1a). VN QDs are found to uniformly disperse on the graphene sheet without aggregation (Fig. 1b), whose cross-section size is quite uniform, ranging from 2 to 3 nm (Fig. 1c). The high-angle annular dark-field scanning transmission electron microscopy (HAADF-STEM) image reveals that the VN QDs have a regular hexagonal structure with the (110) crystal plane on the surface (Fig. 1d). The thickness of the VN QDs is about 0.5–0.6 nm (Fig. 1e and f), equivalent to 4–5 atomic layers. STEM elemental mapping confirms that the QDs are composed of homogeneously dispersed V, N and O elements (Fig. 1g). The existence of the O element indicates the strong interaction between the VN QDs and oxygen. On the other hand, when V_2O_5/GO was treated by ammonization at 800 °C, VN QDs were also gradually formed (Fig. S4†), revealing a spontaneous dispersion phenomenon. The spontaneous dispersion should proceed with diminishing free enthalpy, indicating strong interactions between VN and N-doped graphene.

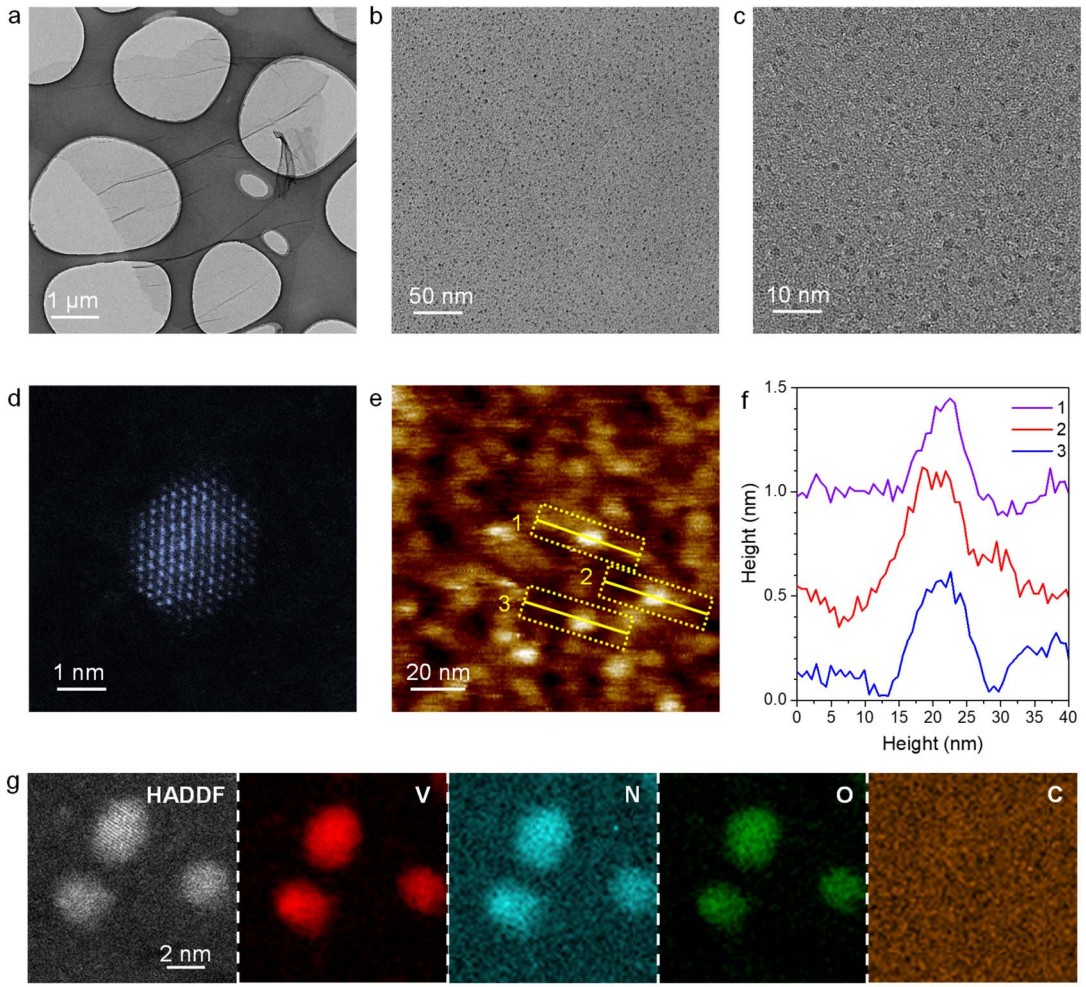

Fig. 1 Characterization of the morphology, structure and elemental composition of VN QDs/rGO. (a and b) TEM and (c) HRTEM images of VN QDs/rGO. (d) High-resolution HAADF-STEM image taken from a single VN QD. (e) Atomic force microscopy (AFM) image and (f) corresponding height profiles of VN QDs/rGO. (g) EDS elemental mapping of V, N, O and C in VN QDs/rGO.

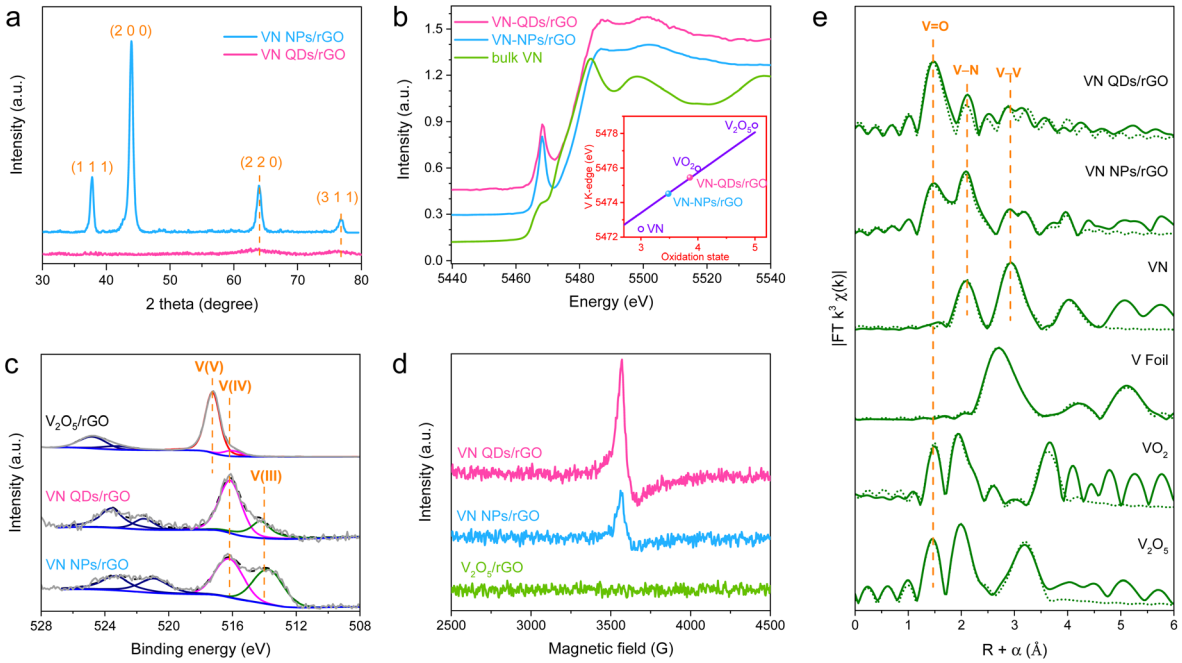

Fig. 2 Characterization of the phase, electronic and coordinate structure of VN QDs/rGO. (a) XRD patterns, (b) V K-edge XANES spectra, (c) high-resolution XPS curves at the V 2p level and (d) ESR spectra of the indicated samples, and (e) FT-EXAFS curves of the samples.

The X-ray powder diffraction (XRD) pattern of VN NPs/rGO (Fig. 2a) displays typical diffraction peaks of the VN phase (JCPDS-35-0768), while that of VN QDs/rGO shows only weak diffractions of the (220) and (311) crystal planes owing to the nano-size of VN QDs. X-ray absorption near-edge structure (XANES) measurements of the catalysts and various references, including V foil, bulk VN, VO_2 and V_2O_5 were carried out to reveal the chemical state of V in VN QDs/rGO (Fig. 2b and S5†). Based on the correlation between the V valence states and the positions of the K-edge in the XANES spectra, we show that the average valence state of V was 3.82 in VN QDs/rGO. The high-resolution X-ray photoelectron spectroscopy (XPS) V 2p curves demonstrate the mixed valence state of V(III) and V(IV) within the VN-based materials (Fig. 2c and S6†). The proportion of V(IV) increases in the order of VN QDs/rGO > VN NPs/rGO > bulk VN (Table S2†), consistent with the electron spin resonance (ESR) spectra (Fig. 2d), which indicates that V(IV) mainly comes from the surface VN_xO_y species. The extended X-ray absorption fine structure analysis (EXAFS) was adopted to identify the coordinate structure of V in the catalysts (Fig. 2e and S7†). The peaks at 2.1 and 2.8 Å are assigned to the scattering of V–N and V–V coordination in VN QDs, referring to the peaks in bulk VN. The peak at 1.5 Å is associated with the V–O bonds, attributed to the surface-adsorbed oxygen as well as the exchange of the surface lattice N with O.[21] XPS studies of N 1s and O 1s levels further confirm the presence of lattice oxygen and adsorbed oxygen on the surface of VN QDs (Fig. S8 and S9†).

Catalytic performance

In the AODS tests, DBT, the richest refractory sulfur-compound in diesel fuel, was selected as a model thiophenic sulfide. Among all the investigated V-based catalysts, VN-QDs/rGO possesses the lowest V content, but shows the best catalytic performance by completing the reaction in 4 h at 100 °C (Fig. 3a). Neat rGO shows negligible catalytic performance, which demonstrates that the V species is the only active site under the current reaction conditions. When the reaction temperature was decreased to 70 °C, VN QDs/rGO was still robust (Fig. 3b), while the performances of VN NPs/rGO and V_2O_5/rGO were almost completely attenuated, demonstrating that VN QDs/rGO possesses a much higher intrinsic activity.

To access the catalytic mechanism, we adopted *in situ* electron spin resonance (ESR) characterization with dimethylpyridine *N*-oxide (DMPO) for spin trapping (Fig. 3c). In two blank tests without the catalyst or O_2, no ESR signal was detected. When O_2 was introduced into the reaction system containing VN-QDs/rGO, an obvious radical signal with six-fold peaks appeared, even at room temperature (25 °C). The signal is assigned to DMPO-O_2^- species ($g = 2.0059$, $A_N = 13.794$ and $A_{\beta H} = 10.221$), indicating that $O_2^{\bullet-}$ was the reactive species in this reaction.[30] The ESR signal intensities follow the order of VN QDs/rGO > VN-NPs/rGO, consistent with the order of their catalytic performances. Radical scavenging experiments were then performed to investigate the involvement of radical species with *tert*-butyl alcohol (TBA) and *p*-benzoquinone (PBQ) as the scavengers for OH and O_2^- radicals, respectively.[31] As summarized in Fig. 3d, the catalytic effect of VN QDs/rGO shows almost no change with the addition of TBA, while it significantly deteriorates with the addition of PBQ, demonstrating that O_2^- is the active species in this reaction.

The catalytic performance of VN QDs/rGO in the AODS of DBT was further evaluated at different temperatures. As

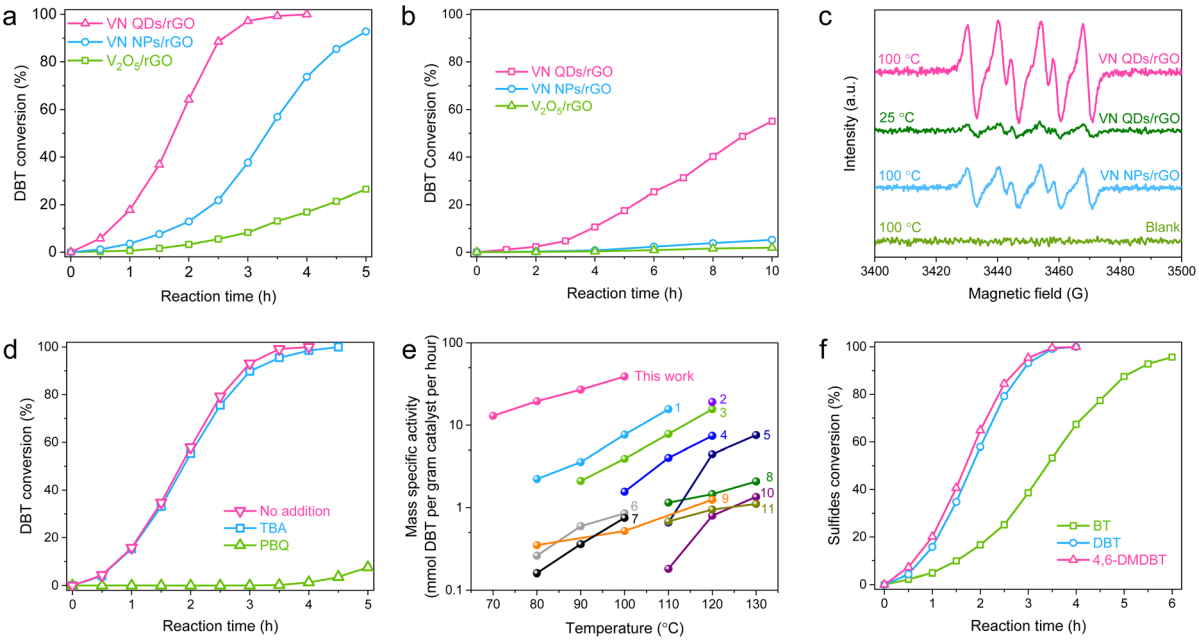

Fig. 3 Evaluation of the catalytic performance of VN QDs/rGO in the AODS reactions. (a and b) Conversion of DBT over the indicated catalysts. Reaction conditions: $m_{catal} = 2$ mg, $V_{oil} = 30$ mL, $F_{air} = 40$ mL min^{-1}. The reaction temperatures were 100 and 70 °C for (a) and (b), respectively. (c) ESR curves of the *in situ* DMPO trapping tests. (d) Reaction efficiency of DBT with the addition of TBA and PBQ. Reaction conditions: $T = 100$ °C, $m_{catal} = 2$ mg, $V_{oil} = 30$ mL, $F_{air} = 40$ mL min^{-1}. (e) Comparison of mass specific activity with those of the state-of-the-art heterogeneous catalysts reported in the literature. (1) CoMo nanosheet;[22] (2) atomic-layered V_2O_5;[9] (3) Co–Ni–Mo–O nanotube;[15] (4) MoO_x/MC-600;[23] (5) 3DOM WO_x;[24] (6) boron nitride nanosheet;[25] (7) Ce–Mo–O;[26] (8) Pt/h-BN;[27] (9) Co–Mo–O;[28] (10) boron carbide nanosheet;[29] (11) V_2O_5/BNNS.[19] (f) Reactivity of different thiophenic sulfides. Reaction conditions: $m_{catal} = 2$ mg, $T = 100$ °C, $V_{oil} = 30$ mL, $F_{air} = 40$ mL min^{-1}.

illustrated in Fig. S10,† VN QDs/rGO is active at a low temperature of 70 °C owing to its excellent capacity for O_2 activation. Compared with the well-known heterogeneous catalysts reported in the literature (Fig. 3e), VN QDs/rGO possesses a higher mass specific activity. The TOF value was determined to be hundreds of times higher than those of the well-known vanadium oxides and V-based polyoxometalates (Table S3†). Based on the conversion curves at different temperatures, reaction kinetics was investigated with a pseudo-first-order kinetic model, and the apparent activation energy (E_a) was calculated to be 72.9 kJ mol^{-1} based on the Arrhenius equation (Fig. S11†).

To verify the versatility of the catalyst, two other typical thiophenic compounds, benzothiophene (BT) and 4,6-dimethyldibenzothiophene (4,6-DMDBT) were adopted in the AODS tests. The reactivity of the three sulfur-compounds followed the sequence of BT < DBT < 4,6-DMDBT (Fig. 3f and S12†), consistent with the order of their valence electron densities of S atoms. The result suggests that the oxidation of thiophene derivatives on VN QDs/rGO conforms to the mechanism of electrophilic addition.[32]

First-principles calculations

VN QDs and plane basal models for four-atom-thick VN on a single-atom graphene sheet were built to gain atomic-level insights into the underlying mechanism. We show that stronger interactions and electron transfer are established between the interface of VN and graphene when N is introduced into the graphene framework (Fig. S13†). The electron density of V sites also increases accordingly, which will raise the donor state of V sites and improve the electron donating capability of V. O_2 adsorption behaviour on VN QDs was then investigated to identify the active sites (Fig. 4a), showing that O_2 molecules tended to be side-on adsorbed on V sites (Fig. S14†), accompanied by charge transfer. The investigated surface, edge and corner sites in the VN QD model all exhibit strong adsorption capacities for O_2 with the adsorption energies of 1.32, 1.59 and 1.88 eV, respectively (Fig. 4b). By contrast, the surface sites of the plane basal models show much lower adsorption energies toward O_2, indicating that bulk VN particles are not good at O_2 activation, consistent with the ESR results. Furthermore, the O–O bond length is stretched to 1.311, 1.325 and 1.344 Å on the surface, edge and corner sites, respectively (Table S4†). Compared with that of O_2^- radicals (1.32 Å[33]), the abundant edge and corner sites of VN QDs appear to better promote the activation and dissociation of O_2 and reason the subsequent reduction of the minimum conversion temperature. Since the O_2 activation performance of a surface depends on its electron donating capacity, work functions (WFs) were calculated, and the WF of the VN QD was found to be distinctly lower than that of the plane basal models, which implies its stronger electron donating capability (Fig. S15†).[34]

The partial density of states (PDOS) results (Fig. 4c) suggest that electrons are transferred from the V atoms to the O_2 $-2\pi_p^*$

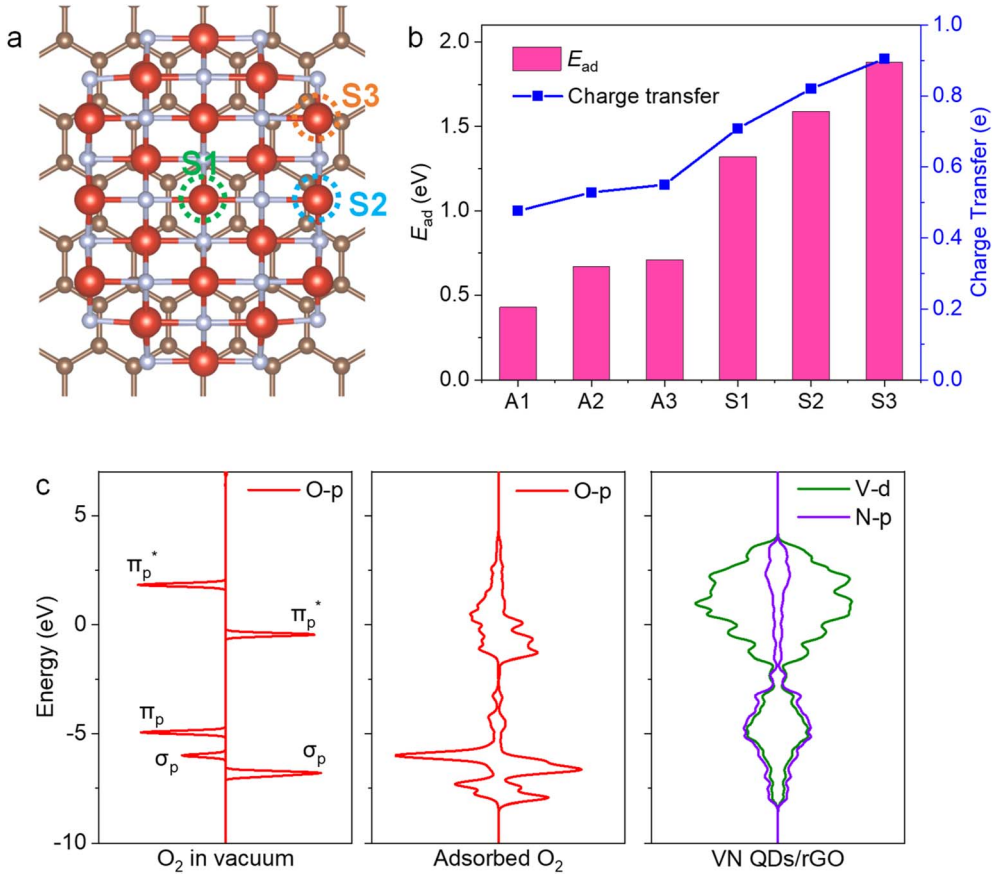

Fig. 4 Investigation of the catalytic mechanism by DFT calculations. (a) Top view of the schematic structure for the four-atom-thick VN QD on a graphene sheet. (b) Adsorption energies and numbers of charge transfer for O_2 adsorbed on different sites. (c) PDOS results of O_2 in a vacuum, adsorbed O_2 and VN QDS/rGO.

orbital. A strong hybridization among V 3d, O_2–2π and O_2–2σ orbitals demonstrates that the chemically inert triplet oxygen was transferred to reactive V–O_2^- species.[35] On the other hand, strong adsorption of DBT is realized by the coordination unsaturated edge and corner V sites *via* the electron electronic coupling of the π orbital of the aromatic ring and the d orbital of the V site, which stretches the C–S bond from 1.745 to 1.767 Å and improves its reaction activity. As a comparison, the adsorption of DBT on the surface site is not permitted due to the lower adsorption energy. The above observations show that the low-coordinated edge/corner V sites, which effectively play a role in both O_2 activation and sulfide adsorption, are the active centers of the AODS reaction with excellent low-temperature catalytic performance. Meanwhile, due to the nano-size of VN QDs, the electronic structure of the edge/corner sites is more readily regulated through the interaction with the carrier, which further enhances the catalytic performance.

Practical performance evaluation

Orienting to the practical performance evaluation, the AODS experiment was conducted on a real diesel at 80 °C, whose sulfur content is 577.6 ± 3.4 ppm. The original sulfides in the diesel are made up of BT, DBT and their derivatives (Fig. S16 and Table S5†). The evolution of sulfur species during the AODS between 0 and 60 min was determined using a gas chromatograph equipped with a flame photometric detector (GC-FPD, Fig. 5a). As the reaction proceeds, the initial peaks are shifted to a longer retention time, assigned to the conversion of thiophenes into sulfones. Nearly all the thiophenes were completely converted at 60 min, confirming the outstanding catalytic activity of VN QDs/rGO. The generated sulfones with strong polarity were then extracted using methanol as a recoverable extractant, which reduced the sulfur content of the diesel to 7.7 ± 0.9 ppm (Table S6†), meeting the most stringent standard in force for transportation fuels. Furthermore, repeated experiments were also conducted with C_2BT to evaluate the desulfurization effect. The conversion of C_2BT showed only a slight decrease in six consecutive repeated runs (Fig. 5b and S17†), mainly caused by the mechanical loss of catalysts. Following the repeated experiments, the recycled catalyst was analyzed by XPS (Fig. 5c). No peak shift was observed, demonstrating the stability of VN QDs/rGO in the AODS of real diesel. Based on such a catalyst with both excellent activity and stability, we demonstrate that the deep desulfurization of diesel could be realized through the AODS process with ultra-high cost efficiency.

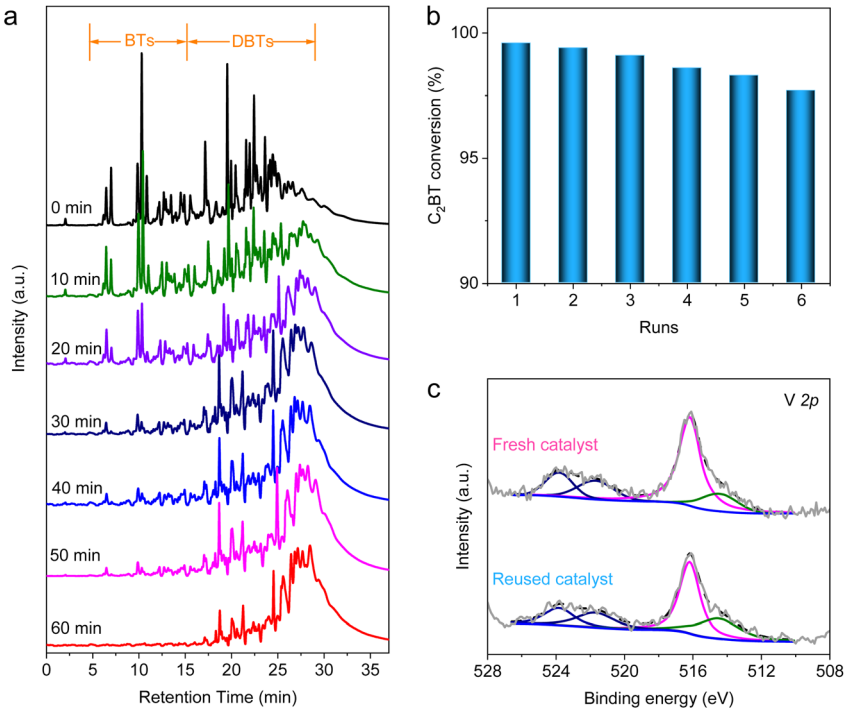

Fig. 5 Practical performance evaluation of VN QDs/rGO in real diesel desulfurization. (a) Chromatograms of the real diesel detected by GC-FPD under different reaction times. Reaction conditions: $T = 80$ °C, $m_{catal} = 20$ mg, $V_{oil} = 30$ mL, $F_{air} = 40$ mL min^{-1}. (b) Reusability of VN QDs/rGO in AODS of diesel with C_2BT as a reference. Reaction conditions: $T = 80$ °C, $m_{catal} = 20$ mg, $V_{oil} = 30$ mL, $F_{air} = 40$ mL min^{-1} (c) V 2p XPS curves of the fresh and recycled catalysts.

Conclusions

In summary, we have proposed a facile method to uniformly anchor VN QDs onto N-doped graphene, controllably creating coordination-unsaturated V sites for the low-temperature AODS of diesel fuel. We show that VN QDs/rGO is two orders of magnitude more active than the reported V-based catalysts in the AODS of DBT, and activates the reaction at 70 °C. By combining systematic characterization and computational studies, we identified that the autogenetic low-coordinated V species accompanied by anion vacancies at the edges and corners of VN QDs have excellent capacity in the activation of both O_2 and sulfides. Meanwhile, VN QDs acquire enhanced electron donor ability for O_2 activation from the interaction with the N-doped graphene carrier, which endows our catalysts with outstanding low-temperature catalytic performance. Stepping further toward the industrial level, VN QDs/rGO achieves full conversion of almost all the sulfides in a real diesel at a low temperature of 80 °C with high durability and extremely low theoretical energy consumption. Further extraction using a solvent enables the desulfurized diesel to meet the strictest fuel standard in force (<10 ppm).

Data availability

The published article includes all datasets generated or analyzed during this study.

Author contributions

S. G. and H. C. supervised the research. H. Y. and S. G. conceived and designed the research project. H. Y. and J. B. carried out the catalyst preparation and AODS experiments. L. B., L. Y., W. W., D. W., and Y. L. performed the characterization of the materials and analyzed the collected data. L. G. and Q. Z. carried out the TEM analyses. H. Y. wrote the original draft. S. G. revised the final manuscript. All authors discussed the results and assisted during manuscript preparation.

Conflicts of interest

There are no conflicts to declare.

Acknowledgements

This research was supported by the National Natural Science Foundation of China (No. 21808098), Natural Science Foundation of Shandong Province (No. ZR2019QB025), Yantai Science and Technology Development Program (No. 2019XDHZ106), and National Science Fund for Distinguished Young Scholars (No. 52025133). The authors would like to thank BSRF, NSRL and SSRF for the synchrotron beam time.

Notes and references

1 Organization of the Petroleum Exporting Countries, in *2020 OPEC World Oil Outlook 2045*, ed. T. Spence and J. Griffin, OPEC, Vienna, Austria, 2020, ch. 2, pp. 50–86.
2 J. Song, Y. Li, P. Cao, X. Jing, M. Faheem, Y. Matsuo, Y. Zhu, Y. Tian, X. Wang and G. Zhu, *Adv. Mater.*, 2019, **31**, 1902444.
3 M. Chi, T. Su, L. Sun, Z. Zhu, W. Liao, W. Ren, Y. Zhao and H. Lü, *Appl. Catal., B*, 2020, **275**, 119134.
4 Z. Jin, L. Wang, E. Zuidema, K. Mondal, M. Zhang, J. Zhang, C. Wang, X. Meng, H. Yang, C. Mesters and F. S. Xiao, *Science*, 2020, **367**, 193–197.
5 P. Y. Xin, J. Li, Y. Xiong, X. Wu, J. C. Dong, W. X. Chen, Y. Wang, L. Gu, J. Luo, H. P. Rong, C. Chen, Q. Peng, D. S. Wang and Y. D. Li, *Angew. Chem., Int. Ed.*, 2018, **57**, 4642–4646.
6 L. N. Cao, W. Liu, Q. Q. Luo, R. T. Yin, B. Wang, J. Weissenrieder, M. Soldemo, H. Yan, Y. Lin, Z. H. Sun, C. Ma, W. H. Zhang, S. Chen, H. W. Wang, Q. Q. Guan, T. Yao, S. Q. Wei, J. L. Yang and J. L. Lu, *Nature*, 2019, **565**, 631–635.
7 L. Nie, D. Mei, H. Xiong, B. Peng, Z. Ren, X. I. P. Hernandez, A. DeLaRiva, M. Wang, M. H. Engelhard, L. Kovarik, A. K. Datye and Y. Wang, *Science*, 2017, **358**, 1419–1423.
8 J. Huang, S. He, J. L. Goodsell, J. R. Mulcahy, W. Guo, A. Angerhofer and W. D. Wei, *J. Am. Chem. Soc.*, 2020, **142**, 6456–6460.
9 C. Wang, H. P. Li, X. J. Zhang, Y. Qiu, Q. Zhu, S. H. Xun, W. S. Yang, H. M. Li, Z. G. Chen and W. S. Zhu, *Energy Fuels*, 2020, **34**, 2612–2616.
10 M. Zhang, J. Liu, H. Li, Y. Wei, Y. Fu, W. Liao, L. Zhu, G. Chen, W. Zhu and H. Li, *Appl. Catal., B*, 2020, **271**, 118936.
11 L. Sun, T. Su, J. Xu, D. Hao, W. Liao, Y. Zhao, W. Ren, C. Deng and H. Lü, *Green Chem.*, 2019, **21**, 2629–2634.
12 Y. Li, J. Song, M. T. Jiang, M. Bawa, X. H. Wang, Y. Y. Tian and G. S. Zhu, *J. Mater. Chem. A*, 2020, **8**, 9813–9824.
13 N. F. Tang, Z. X. Jiang and C. Li, *Green Chem.*, 2015, **17**, 817–820.
14 P. W. Wu, W. S. Zhu, B. L. Dai, Y. H. Chao, C. F. Li, H. P. Li, M. Zhang, W. Jiang and H. M. Li, *Chem. Eng. J.*, 2016, **301**, 123–131.
15 Y. Liu, L. Han, J. Zhang, R. Yao, H. Zhan, H. Yang, L. Bai, L. Yang, D. Wei, W. Wang and H. Chen, *Ind. Eng. Chem. Res.*, 2020, **59**, 6488–6496.
16 Q. Q. Gu, G. D. Wen, Y. X. Ding, K. H. Wu, C. M. Chen and D. S. Su, *Green Chem.*, 2017, **19**, 1175–1181.
17 P. W. Wu, Q. D. Jia, J. He, L. J. Lu, L. L. Chen, J. Zhu, C. Peng, M. Q. He, J. Xiong, W. S. Zhu and H. M. Li, *J. Hazard. Mater.*, 2020, **391**, 122183.
18 Y. Zou, C. Wang, H. Chen, H. Ji, Q. Zhu, W. Yang, L. Chen, Z. Chen and W. Zhu, *Green Energy Environ.*, 2021, **6**, 169–175.
19 C. Wang, Y. Qiu, H. Wu, W. Yang, Q. Zhu, Z. Chen, S. Xun, W. Zhu and H. Li, *Fuel*, 2020, **270**, 117498.
20 C. Wang, W. Jiang, H. X. Chen, L. H. Zhu, J. Luo, W. S. Yang, G. Y. Chen, Z. G. Chen, W. S. Zhu and H. M. Li, *Chin. J. Catal.*, 2021, **42**, 557–562.
21 E. F. de Souza, C. A. Chagas, T. C. Ramalho, V. Teixeira da Silva, D. L. M. Aguiar, R. S. Gil and R. B. de Alencastro, *J. Phys. Chem. C*, 2013, **117**, 25659–25668.
22 Y. Dong, J. Zhang, Z. Ma, H. Xu, H. Yang, L. Yang, L. Bai, D. Wei, W. Wang and H. Chen, *Chem. Commun.*, 2019, **55**, 13995–13998.
23 W. Jiang, J. Xiao, L. Dong, C. Wang, H. P. Li, Y. P. Luo, W. S. Zhu and H. M. Li, *ACS Sustain. Chem. Eng.*, 2019, **7**, 15755–15761.
24 M. Zhang, W. Liao, Y. Wei, C. Wang, Y. Fu, Y. Gao, L. Zhu, W. Zhu and H. Li, *ACS Appl. Nano Mater.*, 2021, **4**, 1085–1093.
25 L. J. Lu, J. He, P. W. Wu, Y. C. Wu, Y. H. Chao, H. P. Li, D. J. Tao, L. Fan, H. M. Li and W. S. Zhu, *Green Chem.*, 2018, **20**, 4453–4460.
26 Y. Shi, G. Liu, B. Zhang and X. Zhang, *Green Chem.*, 2016, **18**, 5273–5279.
27 J. Y. Gu, M. G. Liu, S. H. Xun, M. Q. He, L. L. Wu, L. H. Zhu, X. Y. Wu, W. S. Zhu and H. M. Li, *Mol. Catal.*, 2020, **483**, 110709.
28 Q. Zhang, J. Zhang, H. Yang, Y. Dong, Y. Liu, L. Yang, D. Wei, W. Wang, L. Bai and H. Chen, *Catal. Sci. Technol.*, 2019, **9**, 2915–2922.
29 L. Dai, Y. C. Wei, X. Y. Xu, P. W. Wu, M. Zhang, C. Wang, H. P. Li, Q. Zhang, H. M. Li and W. S. Zhu, *Chemcatchem*, 2020, **12**, 1734–1742.
30 F. Parrino, S. Livraghi, E. Giamello, R. Ceccato and L. Palmisano, *ACS Catal.*, 2020, **10**, 7922–7931.
31 N. Waiskopf, Y. Ben-Shahar and U. Banin, *Adv. Mater.*, 2018, **30**, 1706697.
32 X. Zeng, X. Xiao, Y. Li, J. Chen and H. Wang, *Appl. Catal., B*, 2017, **209**, 98–109.
33 Y. Zhao, B.-T. Teng, X.-D. Wen, Y. Zhao, Q.-P. Chen, L.-H. Zhao and M.-F. Luo, *J. Phys. Chem. C*, 2012, **116**, 15986–15991.
34 M. T. Greiner, L. Chai, M. G. Helander, W.-M. Tang and Z.-H. Lu, *Adv. Funct. Mater.*, 2013, **23**, 215–226.
35 M. Setvin, U. Aschauer, P. Scheiber, Y. F. Li, W. Hou, M. Schmid, A. Selloni and U. Diebold, *Science*, 2013, **341**, 988–991.